RSC Advances

Cite this: *RSC Advances*, 2012, **2**, 11457–11464

www.rsc.org/advances

PAPER

Dithienylthienothiadiazole-based organic dye containing two cyanoacrylic acid anchoring units for dye-sensitized solar cells

G. D. Sharma,*[a] J. A. Mikroyannidis,*[b] M. S. Roy,[c] K. R. Justin Thomas,[d] R. J. Ball[e] and Rajnish Kurchania[f]

Received 7th August 2012, Accepted 19th September 2012
DOI: 10.1039/c2ra21718j

A new dithienylthienothiadiazole-based organic dye (D) was synthesized by a seven-step synthetic route for use as a sensitizer in dye sensitized solar cells (DSSCs). The dye contains a dithienylthienothiadiazole central unit and two cyanoacrylic acid anchoring side groups. Optical and electrochemical properties of D were evaluated. In addition, density functional theory (DFT) and time dependent density functional theory (TD-DFT) calculations were carried out. A favorable electronic excitation from the highest occupied molecular orbital (HOMO) to the lowest unoccupied molecular orbital (LUMO) indicated that the dye can be used as a sensitizer for DSSC applications. The photovoltaic properties of laboratory scale optimized DSSCs sensitized with D showed a power conversion efficiency (PCE) of 4.22%, which was further improved to 5.47% upon the addition of chenodeoxylic acid (CDCA) as a coadsorbant.

Introduction

Since the seminal work reported in 1991 by O'Regan and Grätzel, dye sensitized solar cells (DSSCs) manufactured from mesoporous anatase TiO_2 electrodes have received much attention because they represent a promising alternative to conventional solar cells based on silicon.[1] DSSCs based on polypyridyl Ru complexes have been reported with a high point contact concentrator (PCC) of almost 12% under standard AM1.5 sunlight irradiation.[2] Although polypyridyl Ru dyes have a high power conversion efficiency (PCE) and long-term stability, the large scale application of these dyes has become a critical problem due to limited resources and the costly purification steps required for their manufacture.[3] Fortunately, metal-free dyes could provide a competitive alternative to polypyridyl Ru-based dyes due to their facile modification, high molar coefficient, relatively inexpensive preparation and straightforward compliance with environmentally friendly guidelines.[2c,3] These attributes also make them ideal for solid state DSSCs, utilizing thinner TiO_2 layers. In particular, it is encouraging to note that a promising photon-to-current conversion efficiency of up to 10.3% has been achieved by Wang *et al.*[4] A common strategy in the design of highly efficient metal-free dyes for DSSCs is linking the electron donor and acceptor (D–A) systems through the π-conjugated bridges. Commonly referred to as D-π-A dyes, these systems have been found to possess photoinduced intramolecular charge transfer (ICT) properties,[2c,3] making them suitable for DSSC applications. In recent years, the design and synthesis of D-π-A metal free organic dyes with various donor moieties such as coumarin,[5] indoline,[6] triarylamine,[7] porphyrin,[8] squaraine[9] and amine free heterocycles[10] has led to a number of efficient sensitizers for DSSCs.

Organic dyes generally suffer due to their relatively narrow absorption spectra with very poor absorption in the longer wavelength region. However, to realize large photocurrent responses, a sensitizer must possess a broad absorption extending to the near infrared (NIR) region and the absorption spectrum should overlap with the solar emission spectrum to a large extent. In addition to this, the lowest unoccupied molecular orbital (LUMO) of the dye should lie above the conduction band edge of the TiO_2 semiconductor electrode to favor electron injection in the conduction band of TiO_2. Additionally, the occurrence of the highest occupied molecular orbital (HOMO) of the dye matching with the redox potential of the electrolyte (iodide/tri-iodide) will ensure the regeneration of the dye. Several attempts have been made to fine-tune the above properties in the organic dyes.[7–10]

It was reported by Won *et al.*[11] that the DSSC based on terthiophene containing organic dye with two anchoring acceptor groups exhibited a higher PCE than its counterpart having one anchoring group. The higher PCE observed in the former dye was attributed to the increased amount of dye adsorbed on to the photoanode surface and the presence of

[a]*R & D Centre for Engineering and Science JEC Group of Colleges, JEC Campus, Kukas, Jaipur (Raj), 303101, India. E-mail: sharmagd_in@yahoo.com*
[b]*Chemical Technology Laboratory, Department of Chemistry, University of Patras, GR, 26500, Patras, Greece. E-mail: mikroyan@chemistry.upatras.gr*
[c]*Defence Laboratory, Jodhpur (Raj), 342011, India*
[d]*Organic Materials Laboratory, Department of Chemistry, Indian Institute of Technology, Roorkee, 247667, Uttrakhand, India*
[e]*Department of Architecture and Civil Engineering, University of Bath, Bath, BA2 7AY, UK*
[f]*Department of Physics, Maulana Azad National Institute of Technology (MANIT), 462051, Bhopal (MP(, India*

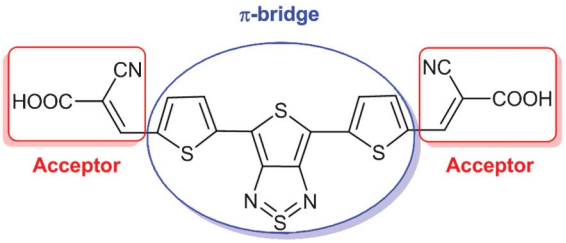

Fig. 1 Chemical structure of dye D.

extended conjugation which reinforced electron transfer in terms of J_{sc}. Similar results were reported by Park *et al.*,[12] for organic dyes with a double electron acceptor anchoring groups on the phenothiazine framework. Yang *et al.* have recently found that dyes based on carbazole and two acceptor anchoring groups (rhodanine-3-acetic acid) are better than the corresponding dye with a single anchoring group. This was attributed to the beneficial retardation of back electron transfer from TiO_2 to the oxidized dye or electrolyte, and enhancement in the charge transfer efficiency in the excited state.[13]

In search of new metal-free sensitizers for DSSCs, we have synthesized a new organic dye (D) featuring two cyanoacrylic acid anchoring groups bridged by a low band gap chromophore, dithienylthienothiadiazole (Fig. 1). Dye D showed a broad absorption band which extended up to approximately 750 nm. The additional acceptor anchoring group in the sensitizer induced a significant influence on the DSSC performance. In particular, the presence of the two anchoring groups is an advantageous feature of dye D, which increased its binding strength on TiO_2. We have investigated the effect of the TiO_2 film thickness on the photoanode and found that the PCE increases from 2.75 to 4.22% as thickness increases from 8 to 12 μm. Any further increase in the TiO_2 film thickness was found to decrease the PCE. The increase in the PCE has been explained with the help of electrochemical impedance spectra (EIS) measurements. The overall PCE value of the optimized DSSCs (12 μm TiO_2 film thickness) sensitized with D was 4.22%, which was further improved to 5.47% following the addition of chenodeoxylic acid (CDCA) as a coadsorbant.

Experimental

Characterization methods

IR spectra were recorded on a Perkin-Elmer 16PC FT-IR spectrometer with KBr pellets. ^{1}H NMR (400 MHz) spectra were obtained using a Bruker spectrometer. Chemical shifts (δ values) are given in ppm with tetramethylsilane as an internal standard.

Synthesis of dye D

A flask was charged with a solution of **6** (see Scheme 1) (0.1202 g, 0.392 mmol) and 2-cyanoacetic acid (0.2000 g, 2.353 mmol) in glacial acetic acid (20 mL). A catalytic amount of ammonium acetate was added to this solution. The solution was stirred and refluxed for 24 h under N_2. The colour of the solution turned red gradually during the heating period. The solution was subsequently concentrated under reduced pressure. Water containing a few drops of hydrochloric acid was added to the concentrate. The precipitate was filtered and washed with water. The crude product was purified *via* silica gel column chromatography to afford a solid with a yield of 0.11 g (57%).

FT-IR (KBr, cm^{-1}): 3500–2800 (OH stretching of carboxylic acid); 2210 (C≡N); 1690 (C=O of carboxylic acid).

^{1}H-NMR (DMSO-d_6) ppm: 8.37 (s, 2H, vinylene); 7.04–6.98 (m, 4H, thiophene). The carboxylic protons were unobserved.

Anal. Calcd for $C_{20}H_8N_4O_4S_4$: C, 48.38; H, 1.62; N, 11.28. Found: C, 47.86; H, 1.90; N, 11.12.

Electrochemical and optical properties

Electrochemical properties of the porphyrin dyes were investigated by cyclic voltammetry (CV) to obtain the HOMO and LUMO levels. The cyclic voltammogram curves were obtained from a three electrode cell in 0.1 M Bu_4NPF_6 acetonitrile solution at a scan rate of 50 mV s^{-1}. The dye coated TiO_2 working electrode, the Pt wire counter electrode and an Ag/AgCl

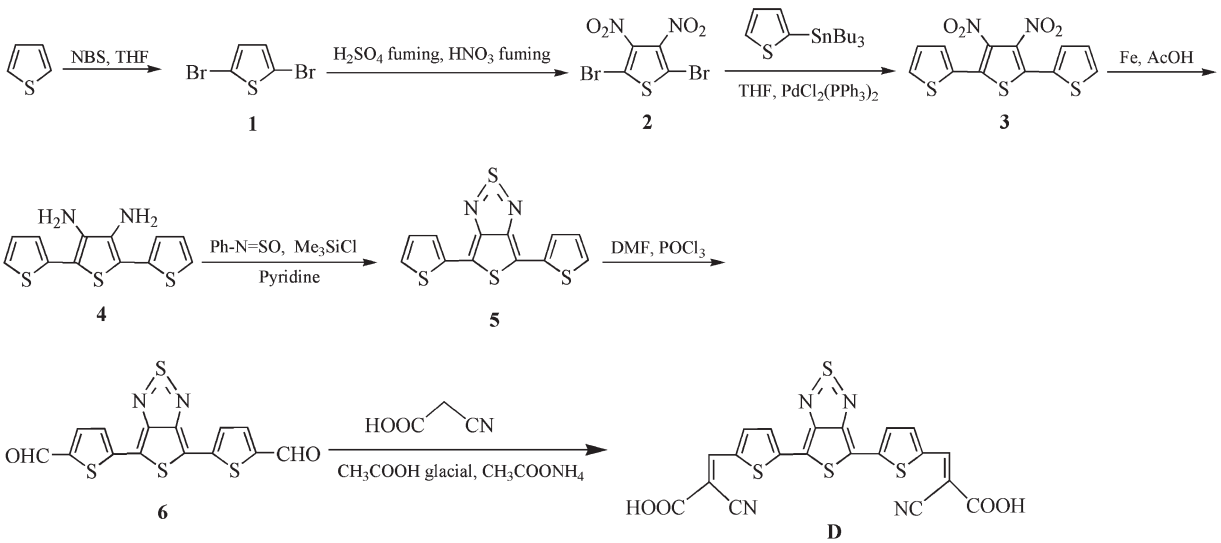

Scheme 1 Synthesis of dye D.

reference electrode were calibrated with ferrocene. All the measured potentials were converted to the NHE (normal hydrogen electrode) scale. The UV-visible absorption spectra of the dye in solution, and adsorbed onto a TiO_2 film, were recorded using a Shimadzu UV-spectrophotometer.

Computational methods

We have performed theoretical calculations, to understand the electronic structure of dye D and to elucidate the origin of possible vertical transitions using the Gaussian 09W[14] (Revision-A.02) program suite. The geometries of the dyes in a vacuum were optimized using density functional theory (DFT) [15] calculations with the hybrid B3LYP[16] density function and the 6-31G** basis set. All optimized geometries were subjected to vibrational analysis, and characterized as a minimum due to the absence of imaginary frequencies. At least 20 vertical excitations to the excited state of the dyes were determined with time-dependent DFT (TD-DFT)[17] calculations using B3LYP or MPW1K[18] density functions. The computations in dimethyl sulfoxide (DMSO) were performed by applying a polarizable continuum model (PCM) employing the integral equation formalism variant (IEFPCM) to describe the electrostatic solute–solvent interactions by the creation of a solute cavity *via* a set of overlapping spheres.[19] The absorption spectra were simulated by using the 20 lowest spin-allowed singlet transitions, mixed Lorentzian-Gaussian lineshape (0.5) and an average full-width at half maximum (3000 cm^{-1}) for all peaks.[20]

Fabrication of DSSCs and characterization

The dye sensitized TiO_2 electrode was prepared using the following method: TiO_2 paste was prepared by mixing 1 g of TiO_2 powder (P_{25}, Degussa, with a crystal structure of 20% rutile and 80% anatase, and a particle size of 20 nm), 0.2 mL of acetic acid and 1 mL of water. Then 60 mL of ethanol was slowly added while sonicating the mixture for 3 h. Finally, Triton X-100 was added and a well dispersed colloidal paste was obtained (TiO_2). The whole procedure is slow under vigorous stirring. The mixture was stirred vigorously for 2–4 h at room temperature and then stirred for 4 h at 100 °C to form a transparent colloidal paste. The TiO_2 paste was deposited on the fluorine-doped tin oxide (FTO) coated glass substrates by the doctor blade technique. The TiO_2 coated FTO films were sintered at 450 °C for 30 min. Before immersing the TiO_2 photoanodes into dye solution, these films were soaked in the 0.2 M aqueous $TiCl_4$ solution for 12 h and washed with deionized water and fully rinsed with ethanol. The films were again heated at a temperature of 450 °C, followed by cooling to room temperature and dipping into a 5×10^{-4} M solution of dye D in DMSO for 12 h at room temperature. To study the effects of chenodeoxylic acid (CDCA) as a coadsorbant on the performance of DSSCs, 10 mM of CDCA was added into the dye solution and then the TiO_2 photoanode was dipped into the solution.

The Pt counter electrodes were prepared by spin-coating drops of H_2PtCl_6 solution onto FTO glass before heating at 350 °C for 15 min. To prevent a short circuit, two electrodes were assembled into a sandwich-type cell with a 20 μm thick spacer. One drop of electrolyte solution LiI (0.05 M), I_2 (0.5 M), dimethyl-propyl-benzimidiazole iodide (DPMII) (0.6 M), and 4-*tert*-butylpyridine (TBP) (0.5 M) in acetonitrile solution was deposited onto the surface of the dye-sensitized TiO_2 electrode and allowed to penetrate inside the TiO_2 *via* capillary action. The Pt coated FTO electrode was then clipped onto the top of the TiO_2 working electrode to form the complete DSSC.

The current density–voltage characteristics (*J–V*) of the devices in darkness and under illumination were measured using a Keithley source meter. A xenon light source coupled with an optical filter provided irradiance (AM 1.5) of 100 mW cm^{-2} at the device surfaces. Photoaction spectra were measured using a monochromator (Spex 500 M, USA) and the resultant photo-current with a Keithley electrometer (model 6514) was interfaced to a computer with LABVIEW software. The electrochemical impedance spectra (EIS) measurements were carried out by applying a bias equivalent to the open circuit voltage (V_{oc}) of the device and recorded over a frequency of 10 mHz to 10^5 Hz with an ac amplitude of 10 mV. The above measurements were recorded with an electrochemical impedance analyser equipped with a frequency response analyser (FRA).

Results and discussion

Synthesis of dye D

Scheme 1 outlines the synthesis of D and its intermediate compounds. In particular, the synthesis of compounds **1–6** has been described in our previous publication.[21] Dye D was prepared by the addition of dialdehyde **6** to an excess of 2-cyanoacetic acid (mol ratio 1 : 6) in glacial acetic acid in the presence of a catalytic amount of ammonium acetate. D was characterized by FT-IR and ^{1}H-NMR spectroscopy.

Table 1 Computed excitation wavelength, oscillator strength, assignment and orbital energies for dye D

Phase	Theory	λ_{max} (nm)	*f*	Assignment	HOMO (eV)	LUMO (eV)	Band Gap (eV)
Vacuum	B3LYP	752	0.775	HOMO → LUMO (100%)	−5.63	−3.94	1.69
		477	0.800	HOMO → LUMO +1 (93%)			
		311	0.160	HOMO − 7 → LUMO (67%) HOMO − 1 → LUMO +1 (24%)			
DMSO	B3LYP	796	1.052	HOMO → LUMO (100%)	−5.49	−3.79	1.70
		494	0.756	HOMO → LUMO +1 (96%)			
		321	0.173	HOMO − 1 → LUMO +1 (69%) HOMO − 5 → LUMO (24%)			
Vacuum	MPW1K	695	0.963	HOMO → LUMO (99%)	−6.39	−3.71	2.68
		408	0.766	HOMO → LUMO +1 (95%)			
		291	0.177	HOMO − 5 → LUMO (93%)			
DMSO	MPW1K	741	1.222	HOMO → LUMO (99%)	−6.27	−3.57	2.70
		421	0.736	HOMO → LUMO +1 (96%)			
		301	0.283	HOMO − 5 → LUMO (94%)			

Theoretical computations

The computed vertical excitation and frontier orbital energies, oscillator strengths for electronic excitations and compositions of vertical transitions, in terms of molecular orbitals of dye D, are given in Table 1. The electronic distributions observed for selected molecular orbitals contributing significantly to the prominent electronic excitations in the dye D are presented in Fig. 2. An absorption peak at *ca.* 700 nm is predicted for D with appreciable oscillator strengths (see Table 1 and Fig. 3). This originates due to the electronic excitation from the HOMO to the LUMO. Since in the HOMO and LUMO levels of the dyes the electronic distribution occurs over the entire molecule, this absorption may be described as a π–π* transition. A second absorption occurring below 500 nm is due to the electronic excitation from the HOMO to LUMO + 1. The position of this peak is insensitive to the number of cyanoacrylic acid units present in the dye. The high value of the oscillator strength for absorption in dye D was attributed to the elongation of conjugation in the dye.

Photophysical and electrochemical properties

Preliminary studies of the photophysical and electrochemical properties of dye D sensitizer were conducted. The normalized optical absorption spectra of this dye in DMSO are shown in Fig. 4. In dilute DMSO solution, the dye D exhibited an absorption band in the shorter wavelength region with an absorption peak around 412 nm. An additional absorption band in the longer wavelength region is shown by an absorption peak at 611 nm. The band centered at 412 nm corresponds to the π–π* transition of the conjugated system, while the band at 611 nm (molar extinction coefficient, 1.27×10^4 M^{-1} cm^{-1}) is assigned to the chemical structure of dithienylthienothiadiazole. The optical band gap (E_{gopt}) estimated from the onset of the absorption edge is 1.67 eV. In the longer wavelength region the absorption band indicates that the number of acceptor groups

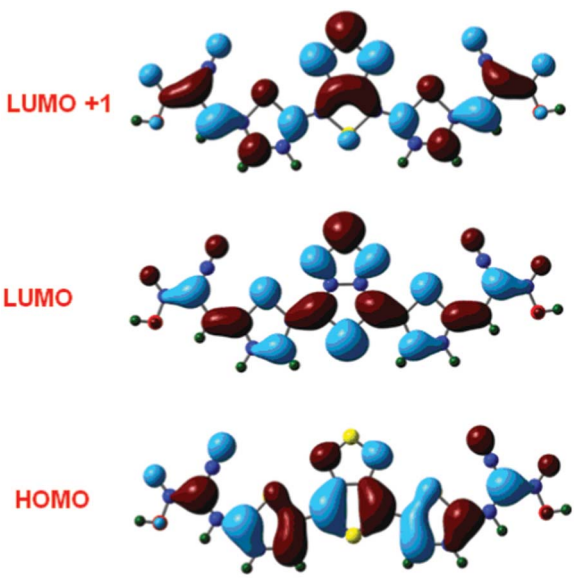

Fig. 2 Electronic distributions in the selected molecular orbitals of dye D.

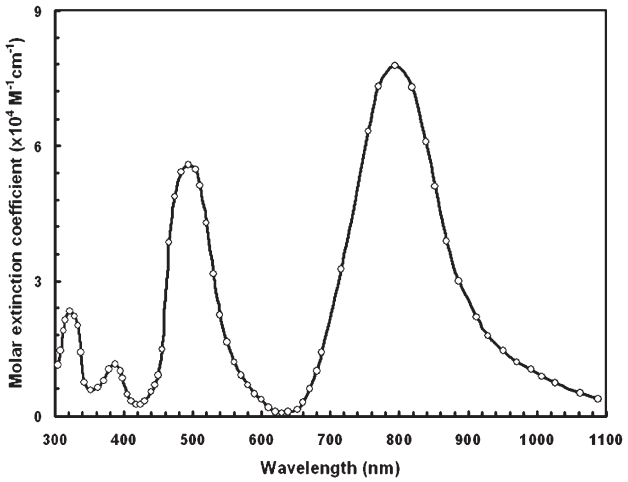

Fig. 3 Simulated (B3LYP/6-31G**) electronic spectra for dye D in DMSO medium.

influences the π–π stacking and also expands the π-conjugation length.[22] This trend in the experimentally observed absorption spectra is closely matched by the theoretically computed spectra. We have also recorded the optical absorption in different solvents and found that the optical absorption band does not have a significant effect.

The absorption spectra of dye D adsorbed onto the TiO_2 film is also shown in Fig. 4 which is red-shifted and broadened compared to those of dyes in solution. Generally, when a sensitizer anchors onto nanocrystalline TiO_2 surfaces, the deprotonation and aggregation of dye molecules affects the optical absorption profiles. Typically the molecular aggregation contains H- and J-aggregates. Deprotonation and H-aggregation always result in a blue-shift of the absorption peak,[23] while J-aggregates mainly lead to a red-shift of the absorption peak. The red-shift and broadening of the absorption band in the absorption spectra on the TiO_2 surface can be attributed to the formation of J-aggregates. Such spectral broadening allows the dye molecules to harvest visible light more efficiently. Since

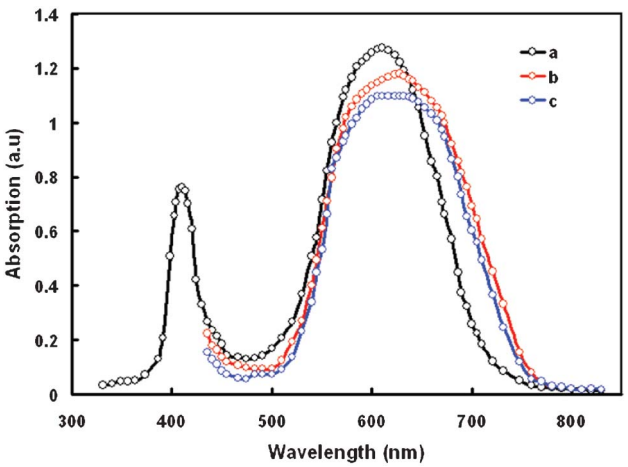

Fig. 4 UV-visible absorption spectra of dye D in (a) DMSO solution; (b) adsorbed onto 8 μm TiO_2 film; and (c) CDCA-D adsorbed on the TiO_2 film.

Table 2 Optical and electrochemical properties of D

E_{gopt}[a] (eV)	E_{ox}[b] (V) *vs.* NHE	E_{red}[c] (V) *vs.* NHE	E_{HOMO} (eV)	E_{LUMO} (eV)	E_{gcv}[d] (eV)
1.67	1.06	−1.0	−5.76	−3.70	1.86 eV

[a] E_{gopt}: the optical band gap value estimated from the onset wavelength in the optical absorption. $E_{gopt} = 1240/\lambda_{onset}$. [b] E_{ox}: the oxidation potential (vs NHE). [c] E_{red}: the reduction potential (vs NHE). $E_{HOMO} = -(E_{ox} + 4.7)$; $E_{LUMO} = -(E_{red} + 4.7)$. [d] E_{gcv}: the electrochemical band gap estimated from cyclic voltammetry.

dye D has two anchoring groups, these may align horizontally next to the TiO_2 surface and thereby slow down the charge recombination.

To evaluate the possibility of electron injection from the LUMO level of dye molecules into the conduction band of TiO_2, the electrochemical redox potentials were measured by cyclic voltammetry (CV) using a three electrode cell and electrochemical analyzer. The redox and oxidation potentials of dye D *vs.* NHE were calibrated by potentials *vs.* Fc^+/Fc and listed in Table 2. The LUMO and HOMO levels of dye D are −1.0 (−3.70 eV) and 1.06 V (−5.76 eV), *vs.* NHE, respectively. These values are very close to the values estimated from the DFT calculations. The value of oxidation potential (1.06 V) is sufficiently more positive than the iodine redox potential (0.4 *vs.* NHE),[23] indicating that the oxidized dyes can be regenerated from the reduced species in the electrolyte to give an efficient charge separation. The reduction potential (−1.0 V) corresponding to the LUMO (−3.7 eV) of dye D is more negative than the conduction band edge of TiO_2 (−0.5 V *vs.* NHE),[23] which provides a sufficient driving force for electron injection. The HOMO level, which corresponds to the oxidation potential, is 1.06 V *vs.* NHE, and is sufficiently more positive than the I_3^-/I^- redox potential (0.4 V *vs.* NHE). This indicates that the oxidized dye, formed after the injection of an electron into the conduction band of TiO_2, could accept the electron from the I^- ion thermodynamically.[24]

To get information about the bonding ability of dye D to the TiO_2 surface, we have measured the FTIR spectra of pure dye and dye adsorbed on to the TiO_2 film. Pure D showed a characteristic peak of C=O in COOH around 1690 cm^{-1}, but this peak disappeared due to deprotonation and new two peaks attributed to the $-COO^-$ group (1592 and 1385 cm^{-1}) were observed for the dye-loaded TiO_2 film.[25] This indicates that there is strong binding and electronic coupling between TiO_2 and dye D.[26]

Photovoltaic properties

Preparation of the TiO_2 film was optimized to obtain a high photovoltaic performance from the DSSC. The thickness of the TiO_2 film is one of the most important factors that affect the performance of DSSCs. The *J–V* characteristics of DSSCs with TiO_2 films having thicknesses of 8, 10, 12, 15 and 18 μm are shown in Fig. 5 and the corresponding photovoltaic parameters are listed in Table 3. An increase in the PCE from 2.76 to 4.18% for the DSSC is observed when the thickness of TiO_2 increases from 4 to 12 μm. Any further increase in the TiO_2 film thickness was found to cause a decrease in the PCE. It has been generally reported that thicker TiO_2 films can adsorb more dye molecules onto their surface.[27] The results indicate that the diffusion length of photo-excited electrons traveling in the TiO_2 particle network

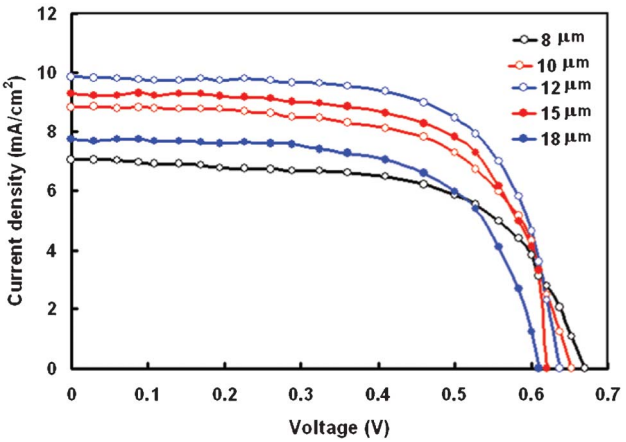

Fig. 5 Current density–voltage (*J–V*) characteristics DSSCs sensitized with dye D under an illumination intensity of 100 mW cm^{-2}, for different thicknesses of TiO_2 film.

is limited to less than around 12 μm. As the electron transporting length becomes longer with the thicker TiO_2 films, this may cause a higher probability of recombination and consequently decreases J_{sc} with a further increase in the thickness of the TiO_2 film. Additionally, thicker TiO_2 films also show a decrease in V_{oc}, which could be attributed to the increasing probability of recombination, owing to the longer electron traveling path. The fill factor (FF) also decreases with increasing thickness of TiO_2 as well, due to the larger series resistance in the thicker TiO_2 film.[28]

Electrochemical impedance spectra (EIS) were used to characterize the charge transport resistance of DSSCs with different thicknesses of TiO_2 film, measured under illumination. The Nyquist plots for the DSSCs are shown in Fig. 6a and the equivalent circuit used to estimate the kinetic parameters is shown in Fig. 7. The Ohmic resistance (R_s) in the equivalent circuit corresponds to the overall series resistance. In general, the EIS of a DSSC measured under illumination shows three semicircles in the range of 10 mHz to 100 KHz. The first semicircle (R_{ct1}) represents the charge transfer resistance at the counter electrode and electrolyte.[29] Charge transfer resistance at

Table 3 Photovoltaic performance of DSSCs based on dye D with different thicknesses of TiO_2 film. The table also shows the values of charge transfer resistances R_{ct1} and R_{ct2}

Thickness (μm)	J_{sc} (mA cm^{-2})	V_{oc} (V)	FF	PCE(%)	R_{ct1}(ohm)	R_{ct2}(ohm)
8	7.07	0.67	0.58	2.75	3.12	31.42
10	8.83	0.65	0.62	3.56	3.18	28.66
12	9.85	0.632	0.68	4.22	3.20	26.58
15	9.28	0.62	0.64	3.68	3.23	28.37
18	7.70	0.61	0.60	2.82	3.19	30.34

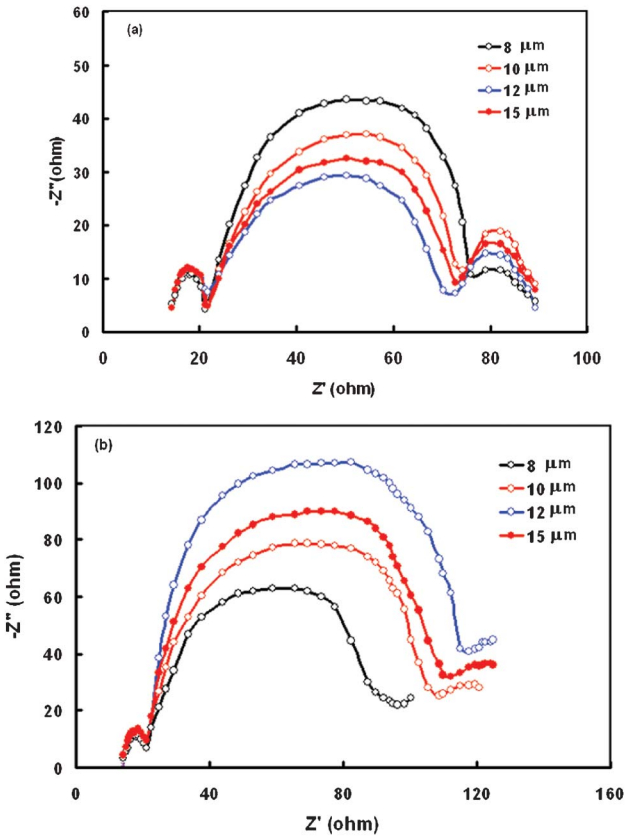

Fig. 6 Nyquist plots of the electrochemical spectra of DSSCs sensitized with dye D measured with an external potential of −0.65 V under (a) illumination and (b) in darkness, for different thicknesses of TiO_2 film.

the TiO_2/dye/electrolyte interface corresponds to the second semicircle (R_{ct2}). In the low frequency (1–0.01 Hz) the range impedance is associated with the Warburg diffusion process of I_3^-/I^- in the electrolyte (Z_w). The values of R_{ct1} and R_{ct2} are summarized in Table 3. The value of R_{ct1} is almost insensitive to the thickness of the TiO_2 film, indicating similar charge transfer resistances at the counter electrode and electrolyte. The value of R_{ct2} decreases with an increase of TiO_2 thickness, resulting in an improved photovoltaic performance. However with further increases in the TiO_2 film thickness above 12 μm, R_{ct2} increases, resulting in reduced photovoltaic performances of DSSCs with thicker TiO_2 films. We have also measured the EIS at an applied voltage equal to the open circuit voltage (V_{oc}) of the DSSC in darkness to investigate the correlation of electron transport with different thicknesses of TiO_2 (Fig. 6b). In these DSSCs, operated in darkness, electron transport though the mesoporous TiO_2, and I^- is oxidized to I_3^- at the counter electrode at the same time.[30] Fig. 6b shows a Nyquist plot of DSSCs with different thicknesses of TiO_2 film, in the dark. The largest circle at the middle frequencies represents the recombination resistance (R_{rec}), *i.e.* resistance for the direct transfer of electrons from the conduction band of TiO_2 to I_3^- at the TiO_2/dye/electrolyte interface or in the electrolyte.[31]

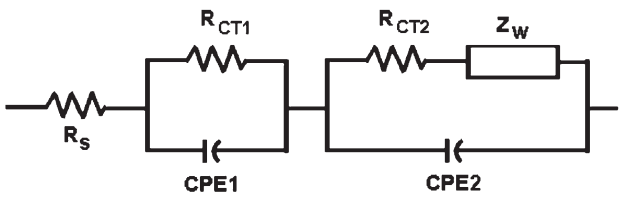

Fig. 7 Equivalent circuit used for fitting the EIS data.

The above results showed that the optimized TiO_2 film thickness for the photoanode is about 12μm. This resulted in the DSSC being optimized by about 4.22% of PCE, which is low due to the dye aggregation at the TiO_2 surface during the sensitization, resulting in a low J_{sc}. When dye is adsorbed onto the TiO_2 surface, π–π stacking of organic dye molecules usually occurs because of the strong intermolecular interactions. Such π–π stacking is advantageous to light harvesting because of its broad feature in the UV-visible absorption spectrum. However, π-stacked aggregation usually has insufficient injection of electrons from the excited state of the dye into the conduction band of TiO_2, which increases the recombination of electrons with oxidized dye molecules. Such recombination leads to a dark current and losses in both J_{sc} and V_{oc}, resulting in a DSSC with a lower PCE.[32,33] Use of an additive in the dye solution can reduce π–π stacking and dye aggregation leading to an improved PCE of the DSSC. Further attempts were made to improve the PCE of the DSSC with a TiO_2 film thickness of 12 μm, and sensitized with dye D using the CDCA as a coadsorbent in the dye solution. The DSSC fabricated with CDCA coadsorbent showed an improved performance with a PCE of 5.46% with J_{sc} = 11.52 mA cm^{-2}, V_{oc} = 0.66 V and FF = 0.72. The values of both J_{sc} and V_{oc} were higher than those without CDCA. This could be the increased competition between the dye and the CDCA molecules for adsorption onto the TiO_2 surface.

The incident photon-to-current conversion efficiency (IPCE) of the DSSCs was estimated to be between 400 and 800 nm according to following expression:

$$\mathrm{IPCE}(\lambda) = 1240 J_{sc}\ (\mathrm{mA\ cm^{-2}})/\lambda(\mathrm{nm}) P_{in}(\mathrm{mW\ cm^{-2}})$$

where λ is the wavelength and P_{in} is the incident radiation per unit area. Fig. 8 compares the IPCE spectra for the DSSCs based on dye D with and without CDCA. It can be seen from this figure that upon the addition of CDCA in the dye solution, the IPCE value was

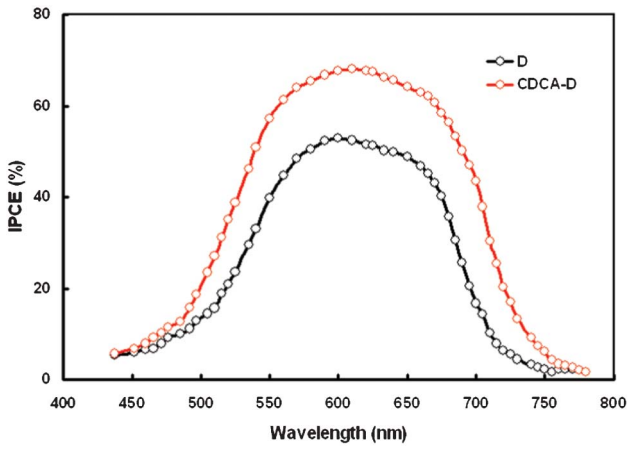

Fig. 8 IPCE spectra for DSSCs sensitized with D and CDCA-D.

enhanced significantly. The maximum IPCE was enhanced from 53 to 68%, when CDCA was incorporated into the dye solution. The IPCE of the DSSC is a product of the light harvesting efficiency (LHE), electron injection efficiency (ϕ_{inj}) and charge collection efficiency (η_{cc}) and expressed as

$$IPCE(\lambda) = LHE(\lambda)x\phi_{inj}x\eta_{cc}$$

The LHE (λ) is the number of absorbed photons per number of incident photons and depends mainly on the amount of dye loading at the photoelectrode surface; ϕ_{inj} is the quantum yield for the electron injection from the dye excited state (LUMO) to the TiO_2 electrode conduction band and η_{cc} is the efficiency of charge collection. We have recorded the UV-visible absorption spectra of CDCA-D adsorbed on the TiO_2 surface and found that with the addition of CDCA in the dye solution, the maximum absorption decreased slightly with slight blue-shift in the absorption peak (as shown in Fig. 4). The amount of dye loading (3.42×10^{-7} mol cm^{-2} for D to 3.22×10^{-7} mol cm^{-2} for CDCA-D) also decreases which indicates that the dye and CDCA compete for the site on the TiO_2 surface in an equilibrium process.[34] The strong interaction between adsorbed dye molecules and oxide molecules in the TiO_2 surface leads to aggregate formation and consequently, a broadening of the absorption spectrum was observed during the dye adsorption on to the TiO_2 surface. This may be attributed to dye–TiO_2 interactions, dye–dye interactions or both. The addition of CDCA in the dye solution diminished these interactions at the TiO_2 surface,[35] leading to a reduction in the dye loading. This means that the LHE was slightly reduced upon the addition of CDCA. Therefore, the IPCE improvement is attributed to the enhancement of electron injection efficiency and/or the charge collection efficiency. After the adsorption of coadsorbant, protons are left on the TiO_2 surface and hence the surface becomes positively charged. This results in a positive shift of the conduction band edge, by the coadsorption of CDCA. The positive shift of conduction band edge enlarges the driving force for electron injection, which results in the enhancement in IPCE and J_{sc}.[36] In addition, the coadsorption also breaks up the dye aggregation and the non-aggregated dye molecules are more favorable for the electron injection, leading to an improvement in J_{sc}.

Since the V_{oc} is theoretically the difference between the quasi-Fermi level of TiO_2 under illumination and the redox potential of the redox couple I_3^-/I^-, the positive shift of the conduction band edge upon adsorption of CDCA will result in a decrease in V_{oc}. However, we observed an increase in V_{oc} after the coadsorption of CDCA. This enhancement is attributed to the suppression of recombination between the injected electrons and I_3^- ion as evidenced from the dark current and EIS spectra. We have observed that the dark current of the DSSC was reduced when CDCA is used as a coadsorbent. Since the dark current is generated due to the recombination of injection electrons and I_3^-, the low value of dark current indicates that the coadsorption of CDCA leads to a suppression of the recombination between injection electrons and I_3^-, which favors the increase in V_{oc}.

The EIS spectra in darkness were also recorded to obtain information about the charge recombination in DSSCs. We observed that the radius of the semicircle in the intermediate frequency region, which represents the electron transfer at the TiO_2/dye/electrolyte interface, increases with coadsorption of CDCA in the dye. A larger radius of this semicircle implies a lower rate of charge recombination between the injected electrons and I_3^-. This also indicates an effective suppression of the back reaction of injected electrons and I_3^- ions. The electron lifetimes (τ_e) in the TiO_2 film, with and without CDCA, were determined from the Bode plots, using $\tau_e = 1/2\pi f_{max}$, where f_{max} is the frequency value of the characteristic low frequency peak in the Bode phase plot. A longer τ_e was found for DSSCs with CDCA in the dye solution, which have smaller f_{max} values than the DSSC without CDCA in the dye solution. This result is in agreement with the higher value of V_{oc} for the DSSC with CDCA added as the coadsorbant into the dye solution.

Conclusions

A new metal-free dye (D) with one dithienylthienothiadiazole central unit and two cyanoacrylic acid anchoring side groups, for use in DSSCs, was synthesized and characterized using optical and electrochemical analysis, and density function theory. The DSSC showed a PCE of 4.22% when the TiO_2 film thickness was 12 μm. This was improved further to 5.47% when the coadsorbant CDCA was added to the solution. The higher values of IPCE for the DSSCs with CDCA, compared to those without CDCA in dye solution, were consistent with the values determined for J_{sc} and PCE. The higher values of recombination resistance and longer electron lifetime determined from the EIS measurements were also consistent with the observed values of J_{sc}, V_{oc} and PCE.

Acknowledgements

The authors (GDS, RK and RJB) wish to thank the UK India Education and Research Initiative (UKIERI II) coordinated by the British Council, New Delhi, India, for financial support through a thematic partnership. RK additionally wishes to thank the Madhya Pradesh Council of Science and Technology, Bhopal, India, for financial support.

References

1 (*a*) B. O'Regan and M. Gratzel, *Nature*, 1991, **353**, 737; (*b*) M. K. Nazeeruddin, A. Kay, I. Rodicio, R. Humphry-Baker, E. Muller, P. Liska, N. Vlachopoulos and M. Gratzel, *J. Am. Chem. Soc.*, 1993, **115**, 6382; (*c*) M. Gratzel, *Acc. Chem. Res.*, 2009, **42**, 1788; (*d*) W. Zhu, Y. Wu, S. Wang, W. Li, X. Li, J. Chen, Z.-S. Wang and H. Tian, *Adv. Funct. Mater.*, 2011, **21**, 756–763; (*e*) J.-L. Bredas, J. E. Norton, J. Cornil and V. Coropceanu, *Acc. Chem. Res.*, 2009, **42**, 1691–1699; (*f*) Y. J. Chang and T. J. Chow, *J. Mater. Chem.*, 2011, **21**, 9523–9531; (*g*) J. He, W. Wu, J. Hua, Y. Jiang, S. Qu, J. Li, Y. Long and H. Tian, *J. Mater. Chem.*, 2011, **21**, 6054–6062; (*h*) S. Mathew and H. Imahori, *J. Mater. Chem.*, 2011, **21**, 7166–7174; (*i*) N. Cai, S.-J. Moon, L. Cevey-Ha, T. Moehl, R. Humphry-Baker, P. Wang, S. M. Zakeeruddin and M. Gratzel, *Nano Lett.*, 2011, **11**, 1452–1456.

2 (*a*) Y. Cao, Y. Bai, Q. Yu, Y. Cheng, S. Liu, D. Shi, F. Gao and P. Wang, *J. Phys. Chem. C*, 2009, **113**, 6290; (*b*) A. Hagfeldt, G. Boschloo, L. C. Sun, L. Kloo and H. Pettersson, *Chem. Rev.*, 2010, **110**, 6595.

3 A. Mishra, M. K. Fischer and P. Bauerle, *Angew. Chem., Int. Ed.*, 2009, **48**, 2474.

4 W. Zeng, Y. Cao, Y. Bai, Y. Wang, Y. Shi, M. Zhang, F. Wang, C. Pan and P. Wang, *Chem. Mater.*, 2010, **22**, 1915–1925.

5 (*a*) Z.S. Wang, Y. Cui, K. Hara, Y. Dan-oh, C. Kasada and A. Shinpo, *Adv. Mater.*, 2007, **19**, 1138–1141; (*b*) Z.S. Wang, Y. Cui, Y.

Danoh, C. Kasada, A. Shinpo and K. Hara, *J. Phys. Chem. C*, 2007, **111**, 7224–7230.
6 (*a*) S. Ito, S. M. Zakeeruddin, R. Humphrey-Baker, P. Liska, R. Charvet, P. Comte, M. K. Zazeeruddin, P. Pechy, M. Tanka, H. Miura, S. Uchida and M. Gratzel, *Adv. Mater.*, 2006, **18**, 1202–1205; (*b*) S. Ito, H. Miura, S. Uchida, M. Takata, K. Sumioka, P. Liska, P. Comte, P. Pechy and M. Gratzel, *Chem. Commun.*, 2008, 5194–5196.
7 (*a*) D. P. Hagberg, T. Edvinsson, T. Marinado, G. Boschloo, A. Hagfeldt and L. Sun, *Chem. Commun.*, 2006, 2245–2247; (*b*) S. Hwang, J. H. Lee, C. Park, H. Lee, C. Kim, C. Park, H. Lee, C. Kim, C. Park, M. H. Lee, W. Lee, J. Park, K. Kim, N. G. Park and C. Kim, *Chem. Commun.*, 2007, 4887–4889; (*c*) A. Baheti, P. Tyagi, K. R. J. Thomas, Y.-C. Hsu and J. T. Lin, *J. Phys. Chem. C*, 2009, **113**, 8541; (*d*) D.P. Hagberg, T. Marinado, K.M. Karlsson, K. Nonomura, P. Qin, G. T. Boschloo, A. Brinck, A. Hagfeldt and L. Sun, *J. Org. Chem.*, 2007, **72**, 9550–9556; (*e*) X. Xu, B. Peng, J. Chen, M. Liang and F. Cai, *J. Phys. Chem. C*, 2008, **112**, 874–880; (*f*) A. Baheti, P. Singh, C.-P. Lee, K. R. J. Thomas and K.-C. Ho, *J. Org. Chem.*, 2011, **76**, 4910–4920; (*g*) L. Y. Lin, C. H. Tsai, K. T. Wong, T. W. Huang, L. Hsieh, S. H. Liu, H. W. Lin, C. C. Wu, S. H. Chou, S. H. Chen and A. I. Tsai, *J. Org. Chem.*, 2010, **75**, 4778–4785; (*h*) P. Shen, Y. Liu, X. Huang, Z. Zhao, N. Xiang, J. Fei, L. Liu, X. Wang, H. Huang and S. Tan, *Dyes Pigm.*, 2009, **83**, 187–197; (*i*) H. Chen, H. Huang, X. Huang, J. N. Clifford, A. Forneli, E. Palomares, X. Zheng, L. Zheng, X. Wang, P. Sen, B. Zhao and S. Tan, *J. Phys. Chem. C*, 2010, **114**, 3280–3286; (*j*) W. Zhu, Y. Wu, S. Wang, W. Li, X. Li, J. Chen, Z. S. Wang and H. Tian, *Adv. Funct. Mater.*, 2011, **21**, 756–763; (*k*) J. Tang, W. Wu, J. Hua, J. Li, X. Li and H. Tian, *Energy Environ. Sci.*, 2009, **2**, 982–990; (*l*) J. Tang, J. Hua, W. Wu, J. Li, Z. Jin, Y. Long and H. Tian, *Energy Environ. Sci.*, 2010, **3**, 1736–1745; (*m*) K. R. J. Thomas, N. Kapoor, C.-P. Lee and K.-C. Ho, *Chem.–Asian J.*, 2012, **7**, 738–750.
8 (*a*) Y. Liu, N. Xiang, X. Feng, P. Shen, W. Zhou, C. Weng, B. Zhao and S. Tan, *Chem. Commun.*, 2009, 2499–2501; (*b*) T. Bessho, S. M. Zakeeruddin, C. Y. Yeh, E. W. G. Diau and M. Grätzel, *Angew. Chem., Int. Ed.*, 2010, **49**, 6646–6649.
9 (*a*) J. Y. Li, C. Y. Chen, C. P. Lee, S. C. Chen, T. H. Lin, H. H. Tsai, K. C. Ho and C. G. Wu, *Org. Lett.*, 2010, **12**, 5454; (*b*) H. Choi, J. J. Kim, K. Song, J. Ko, M. K. Nazeeruddin and M. Gratzel, *J. Mater. Chem.*, 2010, **20**, 3280; (*c*) S. Paek, H. Choi, C. Kim, N. Cho, S. So, K. Song, M. K. Nazeeruddin and J. Ko, *Chem. Commun.*, 2011, **47**, 2874.
10 (*a*) A. Bolag, J. I. Nishida, K. Hara and Y. Yamashita, *Chem. Lett.*, 2011, **40**, 510; (*b*) D. Kumar, K. R. J. Thomas, C.-P. Lee and K.-C. Ho, *Org. Lett.*, 2011, **13**, 2622; (*c*) S. Franco, J. Garin, N. M. De Baroja, R. Perez-Tejada, J. Orduna, Y. Yu and M. Lira-Canto, *Org. Lett.*, 2012, **14**, 752; (*d*) H. Y. Yang, Y. S. Yen, Y. C. Hsu, H. H. Chou and J. T. Lin, *Org. Lett.*, 2010, **12**, 16.
11 Y. S. Won, Y. S. Yang, J. H. Kim, J. H. Ryu, K. K. Kim and S. S. Park, *Energy Fuels*, 2010, **24**, 3676.
12 S. S. Park, Y. S. Won, Y. C. Choi and J. H. Kim, *Energy Fuels*, 2009, **23**, 3732.
13 C. H. Yang, S. H. Liao, Y. K. Sun, Y. Y. Chaung, T. L. Wang, Y. T. Shien and W. C. Lin, *J. Phys. Chem. C*, 2010, **114**, 21786.
14 M. J. Frisch, G. W. Trucks, H. B. Schlegel, G. E. Scuseria, M. A. Robb, J. R. Cheeseman, G. Scalmani, V. Barone, B. Mennucci, G. A. Petersson, H. Nakatsuji, M. Caricato, X. Li, H. P. Hratchian, A. F. Izmaylov, J. Bloino, G. Zheng, J. L. Sonnenberg, M. Hada, M. Ehara, K. Toyota, R. Fukuda, J. Hasegawa, M. Ishida, T. Nakajima, Y. Honda, O. Kitao, H. Nakai, T. Vreven, J. A. Montgomery Jr., J. E. Peralta, F. Ogliaro, M. Bearpark, J. J. Heyd, E. Brothers, K. N. Kudin, V. N. Staroverov, R. Kobayashi, J. Normand, K. Raghavachari, A. Rendell, J. C. Burant, S. S. Iyengar, J. Tomasi, M. Cossi, N. Rega, N. J. Millam, M. Klene, J. E. Knox, J. B. Cross, V. Bakken, C. Adamo, J. Jaramillo, R. Gomperts, R. E. Stratmann, O. Yazyev, A. J. Austin, R. Cammi, C. Pomelli, J. W. Ochterski, R. L. Martin, K. Morokuma, V. G. Zakrzewski, G. A. Voth, P. Salvador, J. J. Dannenberg, S. Dapprich, A. D. Daniels, Ö. Farkas, J. B. Foresman, J. V. Ortiz, J. Cioslowski and D. J. Fox*Gaussian 09, Revision A.02*, Gaussian, Inc., Wallingford CT, 2009.
15 (*a*) W. Kohn and L. J. Sham, *Phys. Rev.*, 1965, **140**, A1133–A1138; (*b*) R. G. Parr and W. Yang, *Density-functional theory of atoms and molecules*, Oxford University Press, Oxford, 1989.
16 (*a*) C. Lee, W. Yang and R. G. Parr, *Phys. Rev.B*, 1988, **37**, 785–89.
17 F. Furche and R. Ahlrichs, *J. Chem. Phys.*, 2002, **117**, 7433–7447.
18 B. J. Lynch, P. L. Fast, M. Harris and D. G. Truhlar, *J. Phys. Chem. A*, 2000, **104**, 4811–4815.
19 (*a*) M. Cossi, V. Barone, R. Cammi and J. Tomasi, *Chem. Phys. Lett.*, 1996, **255**, 327–335; (*b*) J. Tomasi, B. Mennucci and R. Cammi, *Chem. Rev.*, 2005, **105**, 2999–3093.
20 (*a*) S. I. Gorelsky, *SWizard program*http://www.sg-chem.net/, University of Ottawa, Ottawa, Canada, 2010; (*b*) S. I. Gorelsky and A. B. P. Lever, *J. Organomet. Chem.*, 2001, **635**, 187–196.
21 J. A. Mikroyannidis, D. V. Tsagkournos, S. S. Sharma, Y. K. Vijay and G. D. Sharma, *J. Mater. Chem.*, 2011, **21**, 4679.
22 Y. S. Won, Y. S. Yang, J. H. Kim, J. H. Ryu, K. K. Kim and S. S. Park, *Energy Fuels*, 2010, **24**, 3676.
23 (*a*) H. Hara, Z. S. Wang, T. Sato, A. Furube, R. Katoh, H. Sugihara, Y. Dan-oh, C. Kasada, A. Shinpo and S. Suga, *J. Phys. Chem. B*, 2005, **109**, 15476; (*b*) D. Kim, J. K. Lee, S. O. Kang and J. Ko, *Tetrahedron*, 2007, **63**, 1913; (*c*) S. Kim, J. K. Lee, S. O. Kang, J. Ko, J. H. Yum, S. Fantacci, F. Md. D. DeAngelis, M. K. Nazeeruddin and M. Gratzel, *J. Am. Chem. Soc.*, 2006, **128**, 16701; (*d*) D. Hagberg, J. H. Yum, H. Lee, F. D. Angelis, T. Marinado, K. M. Karison, R. Humphry-Baker, L. Sun, A. Hagfedt, M. Gratzel and M. K. Nazeeruddin, *J. Am. Chem. Soc.*, 2008, **130**, 6259.
24 (*a*) C. Klein, M. K. Nazeeruddin, D. D. Censo, P. Liska and M. Grätzel, *Inorg. Chem.*, 2004, **43**, 4216–4226; (*b*) Y. J. Chang and T. J. Chow, *Tetrahedron*, 2009, **65**, 9626–9632.
25 G. Socrates, *Infrared characteristics group frequencies*, 2nd addition Ed; wiely & sons Ltd, Baffins Lane, Chichester, UK, 1994.
26 (*a*) H. N Tian, X. C. Yang, R. K. Chen, R. Zhang, A. Hagfeldt and L. C. Sunt, *J. Phys. Chem. C*, 2008, **112**, 11023; (*b*) M. K.; Nazeeruddin, R. Humphry-Baker, P. Liska and M. Gratzel, *J. Phys. Chem. B*, 2003, **107**, 8981.
27 (*a*) C. Y. Huang, Y. C. Hsu, J. G. Chen, V. Suryanarayanan, K. M. Lee and K. C. Ho, *Sol. Energy Mater. Sol. Cells*, 2006, **90**, 2391–2397; (*b*) J. G. Chen, C. Y. Chen, S. J. Wu, J. Y. Li, C. G. Wu and K. C. Ho, *Sol. Energy Mater. Sol. Cells*, 2008, **92**, 1723–1727.
28 T. Miyssaka, A. Ikegami and Y. Kijitori, *J. Electrochem. Soc.*, 2007, **154**, A455–A461.
29 (*a*) H. G. Yun, Y. Jun, J. Kim, B. S. Bae and M. G. Kang, *Appl. Phys. Lett.*, 2008, **93**, 133311; (*b*) H. G. Yun, B. S. Bae and M. G. Kang, *Adv. Energy Mater.*, 2011, **1**, 337–342; (*c*) J. Bisquert, *Phys. Chem. Chem. Phys.*, 2003, **5**, 5360; (*d*) J. Bisquert, A. Zaban, M. Greenshtein and I. Mora-Sero, *J. Am. Chem. Soc.*, 2004, **126**, 13550.
30 Q. Wang, J. E. Moser and M. Gratzel, *J. Phys. Chem. B*, 2005, **109**, 14945–14953.
31 T. Hashikawa, M. Yamade, R. Kikuchi and K. Eguchi, *J. Electrochem. Soc.*, 2005, **152**, E68–E73.
32 (*a*) A. C. Khazraji, S. Hotchandani, S. Das and P. V. Kamat, *J. Phys. Chem. B*, 1999, **103**, 4693–4700; (*b*) A. Kay and M. Gratzel, *J. Phys. Chem.*, 1993, **97**, 6272–6277.
33 (*a*) X. M. Ren, Q. Y. Feng, G. Zhou, C. H. Huang and Z. S. Wang, *J. Phys. Chem. C*, 2010, **114**, 7190–7195; (*b*) N. R. Neale, N. Kopidakis, J. Van de Lagemaat, M. Gratzel and A. J. Frank, *J. Phys. Chem. B*, 2005, **109**, 23183.
34 Z. S. Wang and G. Zhou, *J. Phys. Chem. C*, 2009, **113**, 15417–15421.
35 (*a*) K. M. Lee, V. Suryanaryanan, K. C. Ho, K. R. J. Thomas and J. T. Lin, *Sol. Energy Mater. Sol. Cells*, 2007, **91**, 1426; (*b*) M. C. Bernard, H. Cachet, P. Falares, A. Hogot-Le Goff, M. Kalbac, I. Lukes, N. J. Oanh, T. Stergiopoulos and I. Arabatzis, *J. Electrochem. Soc.*, 2003, **150**, 155; (*c*) S. Qu, W. Wu, J. Huo, C. Kong, Y. Long and H. Tian, *J. Phys. Chem. C*, 2010, **114**, 1343.
36 D. Kuang, S. Ito, B. Wenger, C. Klein, J. E. Moser, R. Humphry-Baker, S. M. Zakeeruddin and M. Gratzel, *J. Am. Chem. Soc.*, 2006, **128**, 4146.

